JOURNAL OF MATERIALS SCIENCE 30 (1995) 2083–2090

Real time study of failure events in polymers

Part II *Influence of polycarbonate–polyester morphology on the failure micromechanisms*

E. G. RIGHTOR, K. SEHANOBISH, G. P. YOUNG, J. C. CONBOY, J. W. WILCHESTER, C. P. BOSNYAK
Dow Chemical, Building B-1225, Freeport, TX 77541, USA

Real time observations of submicrometre scale failure mechanisms of injection moulded multiphase blends are extremely difficult to perform. This has been accomplished using a specially designed tensile fixture and sample preparation techniques for a polycarbonate–polyester blend. Blunt or sharp cracks could be developed in the blend which were dependent on the shape of the polyester domains. Their initiation and propagation mechanisms have been examined at the submicrometre and bulk scales. The failures observed in the thin-sections were similar to failure mechanisms observed in the bulk.

1. Introduction

Polymer blend components are typically selected to combine the desirable attributes of individual components, such as processability and toughness, with chemical or heat resistance and cost. A good example of this is the development of poly(bisphenol A carbonate), PC, blends with poly(ethylene terephthalate), PET, for engineering applications, such as power tool housings. A key to successful commercial application of this blend lies in understanding the hierarchical structure–property relationships, particularly the development of structure during processing and its subsequent resistance to cracking under impact or fatigue. The focus of this paper is the identification of the submicrometre scale mechanisms and sequence of failure in injection moulded PC–PET blends.

A particular challenge with PC–PET blends is that minor additions of PET to PC result in decreased toughness [1, 2]. Hence, impact modifiers such as core–shell latex rubbers are usually added [1]. In some cases the blend system may not be tough, even with considerable amounts of an impact modifier, unless the PC and polyester phases are finely dispersed at the micrometre size level, or less [3, 4]. Yet, efficient dispersion of PET is challenging due to a very complex hierarchy of morphologies arising from the injection moulding melt flow fields, polymer–polymer interactions and the possibility of crystallization of the polyester phase in injection moulded parts. An excellent review of these problems is presented by Utracki [5]. The influence of the elongated PET domains, that often result from injection moulding on crack propagation, is of special interest as PC toughness is dependent on the shape of modifiers [6]. Due to the anisotropy of blend morphology in injection moulded parts, the fatigue crack resistance also has directional dependence in various PC blends [7].

Transmission electron microscopy (TEM) has been utilized to study the dispersion of components, such as the polyester in PC blends. However, the sample preparation methods of post-mortem fixing of the crack [8], impregnation [9], casting of thin films [10] or drawing of thin films from solution [11–14] do not allow real time study of the morphological response in a moulded specimen. Thus, there is little direct information about the sequence, magnitude, and mechanism of submicrometre failure initiation and propagation in polymer blends.

Electron microscopy has been the mainstay of many previous studies of failure processes, but difficulties in specimen preparation have prevented real time studies on bulk samples with the resolution needed to quantify the influence of morphology on failure events. Submicrometre failure events associated with crack propagation in PC–PET can now be examined using a new sample holder grid design mounted in the TEM. The ability to record the sequence, magnitude and variability of these events on thin sections of bulk polymers processed via actual commercial equipment is important in developing our understanding of failure processes. Additionally, the correlation of these events to failure processes that occur in much thicker, bulk samples is necessary to validate the relevance of the *in situ* TEM technique. In this paper, submicrometre failure events are established for PC–PET by *in situ* TEM studies and their correlation to post-mortem analyses of events that occur in bulk tested parts.

0022–2461 © *1995 Chapman & Hall*

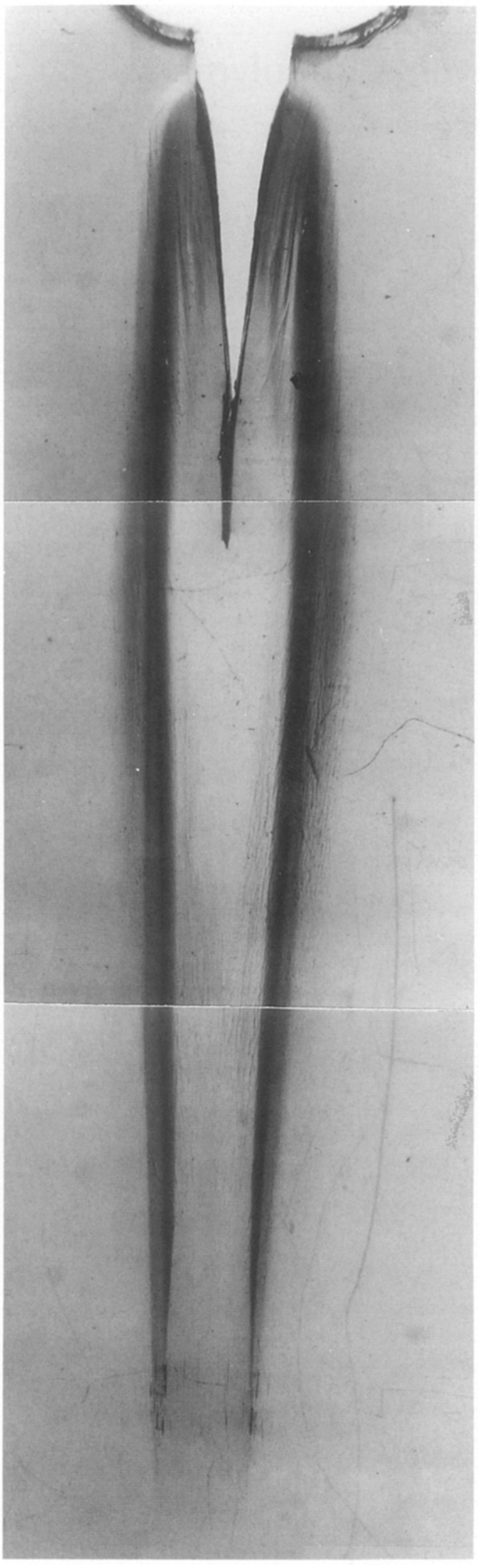

2. Experimental procedure

Materials used in this study were PC of molecular weight, 26 500 g mol^{-1} and a commercially available PET of M_W 104 000 g mol^{-1}. All materials were carefully dried before melt fabrication. The PC and PET were melt mixed in a 30 mm Werner–Pfliederer twin screw extruder at 275 °C in the ratio 80/20 w/w, respectively. The strands were pelletized, dried carefully and injection moulded into plaques of dimensions of 152.4 × 76.2 × 3.175 mm. Injection moulding temperatures were: barrel, 275 °C; mould, 85 °C. Molecular weight analyses of the polycarbonate after injection moulding revealed little change due to the thermal histories.

The plaques were microtomed parallel or perpendicular to the injection melt flow using a Reichert–Jung ultracut E ultramicrotome at 25 °C with a diamond knife. Additional details are given in [15]. Sections were transferred to copper tensile grids in the selected orientation. The PET domains were imaged distinctly without staining for tensile studies. *In situ* TEM tensile experiments on thin-sections sliced from bulk specimens were performed in a Jeol 2000 FX TEM, using a Jeol tensile holder (model EM-SEH). Real time events were recorded on video tape with some static TEM photos being taken prior to and after tensile pulls.

Two types of experiments were planned for the tensile fracture study of the bulk specimen. In approach I, the load was applied remotely, while in approach II, the load was applied at the crack face. Approach II was designed to stop a more brittle failure before it had gone completely through the sample. Both ductile and brittle crack growth situations are commonly encountered in real part failure. The purpose of the two approaches was to determine the correspondence between bulk failure and the submicrometre failure process studied via TEM. The bulk sample dimensions were chosen to match those of sections studied by *in situ* TEM as closely as possible.

2.1. Approach I

Sample bars were made with a length of 152 mm, a width of 51 mm and a thickness of 6 mm. A hemispherical groove was made at one edge of the sample bar, oriented perpendicular to injection moulding flow. A razor notch was placed at the front of the groove so as to resemble the geometry utilized for TEM sample preparation. A groove of 5 mm length and 6 mm width was made into the edge of the sample. The razor sharpened crack extended another 2 mm into the sample. The crack was then remotely loaded in tension at 15 mm s^{-1} in a gear driven Instron (model 1125) with a gauge length of 102 mm. Fig. 1 displays an optical micrograph of the damage zone ahead of the crack in a sample showing considerable ductility.

Figure 1 Optical micrograph of the damage zone produced in a PC–PET sample having the initial dimensions described in the experimental section (approach I).

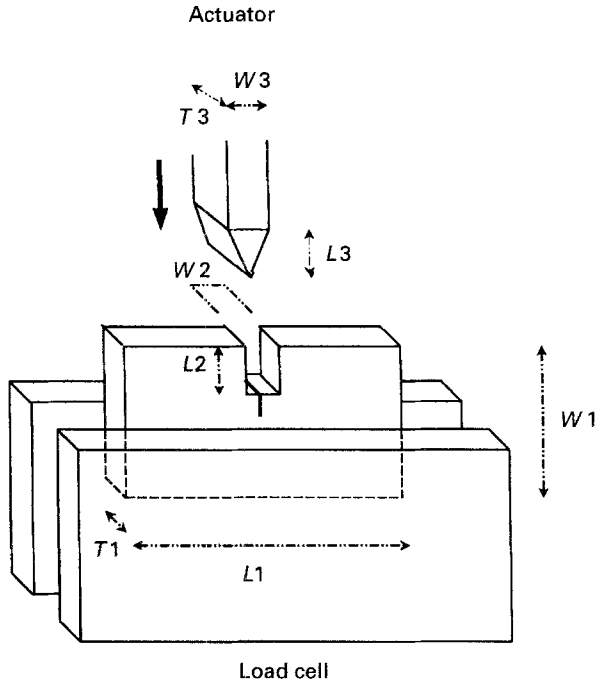

Figure 2 Sketch of the setup used to stop a quickly moving crack before total failure in the PC–PET bulk sample using a wedge technique (approach II), where width, W, equals (1) 5.1, (2) 0.2, (3) 0.6 cm, respectively; length, L, equals (1) 6.35, (2) 1.3, (3) 1.6 cm, respectively; and thickness, T, equals (1) 0.3 and (2) 1.3 cm, respectively.

2.2. Approach II

Coupons of approximately 51 mm width, 64 mm length and 3.2 mm thickness were machine notched (Micromatic model WMSA1018 wet saw). They were then razor notched an additional 2 mm. The samples were placed in a small vise, and the sides of the vise were used as a guide to keep the coupon from leaning during wedge penetration. This setup is illustrated in Fig. 2. A wedge was machined in-house that tapers from 6.4 mm to a point, over a distance of 16 mm. This wedge was used to control the loading, so that it could be rapidly loaded and immediately unloaded when a fast crack began to move, i.e. pulse mode. During wedge loading care was taken so that the apex of the wedge did not reach the crack tip.

The testing was performed on an MTS model 831 Elastomer servohydraulic system. A 8.9 kN load cell was used in range two (2.2 kN full scale). The ramp rate for the wedge was 96.5 mm s^{-1}. For samples with the crack oriented perpendicular to the flow direction, cracks could be stopped using the wedge. However, attempts to stop the crack were unsuccessful when the crack was initiated parallel to the injection moulding direction. The crack tip damage was analysed by post-mortem TEM analysis on these bulk samples.

The razor notched regions of bulk tested PC–PET samples were isolated by cutting with a diamond saw, followed by a jeweller's saw. These pieces were then embedded in epoxy and trimmed for cryomicrotomy. Experience with similar PC blends has shown negligible damage to the PC upon embedding with D.E.R.* 331 epoxy resin, compared with the crack damage itself so this epoxy was used for the present study. The crack arrest region was oriented for sectioning in the crack plane, parallel to the long axis of the sample. Thin-sections, ~ 100 nm thick, were microtomed with a diamond knife at room

* Trademark of The Dow Chemical Company.

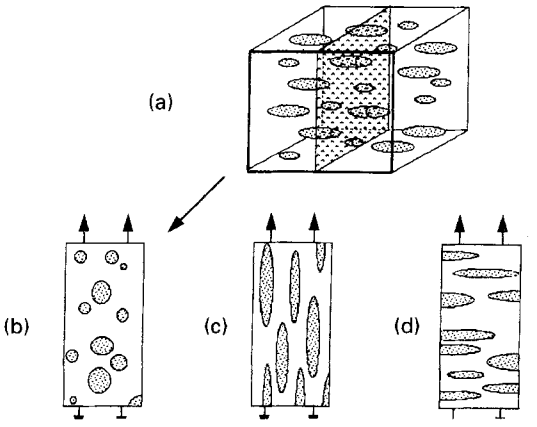

Figure 3 Schematic showing morphology of PC–PET (a) in the injection moulded part and in sections cut perpendicular (b) or parallel to flow (c,d). The shadowed plane shows the sectioning plane for sections cut perpendicular to flow.

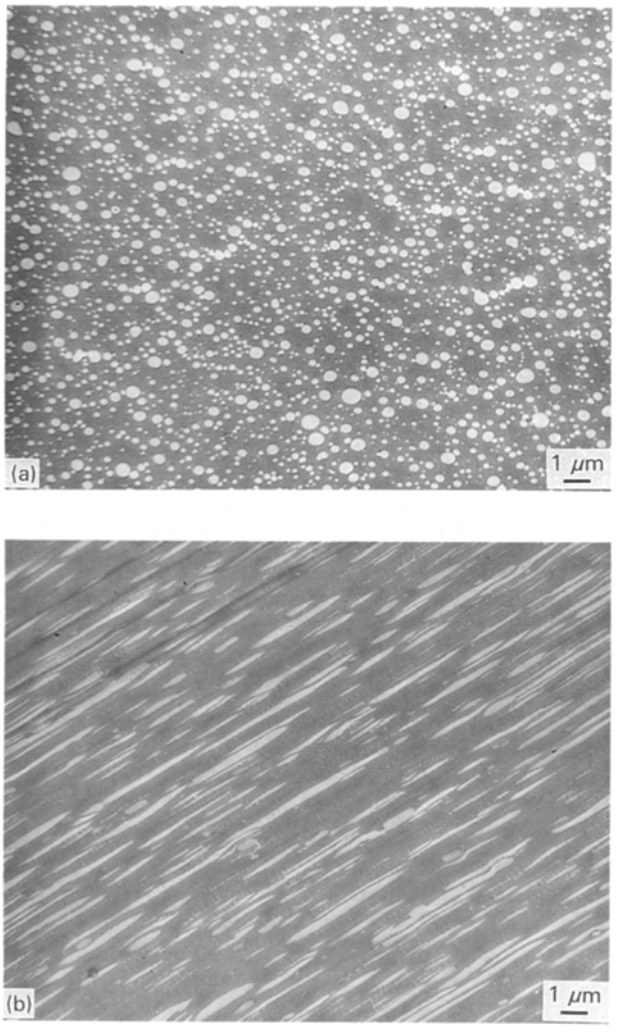

Figure 4 TEM micrograph of PC–PET, microtomed (a) perpendicular to flow showing disc-like PET domains, and (b) parallel to flow showing mainly rod-shaped PET domains. In these micrographs the PC matrix (dark) was stained with RuO_4 for clarity.

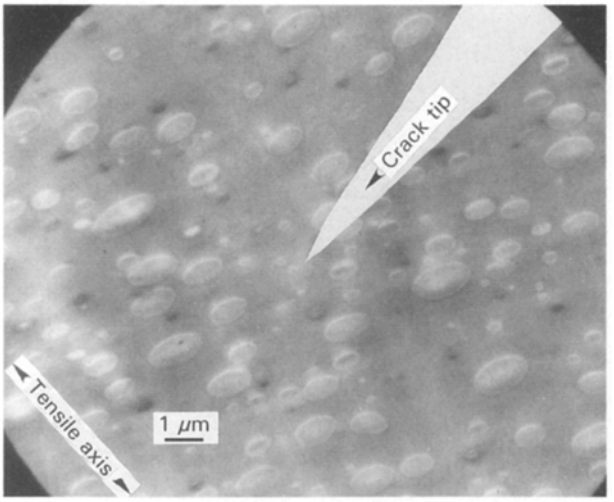

Figure 5 TEM micrograph of crack progressing straight through PET domains when an exceptionally sharp crack is propagating.

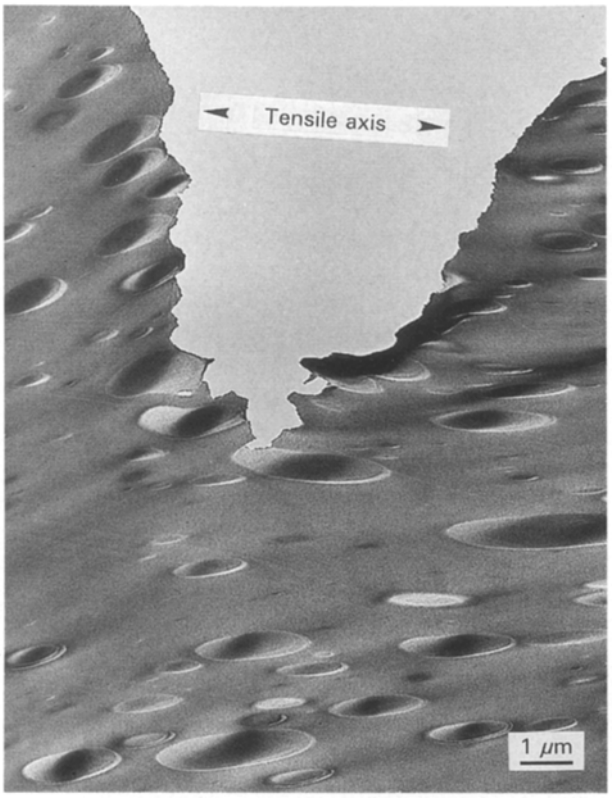

Figure 6 TEM micrograph of crack progressing around PET domains when a blunt crack is propagating.

temperature on a Reichert–Jung ultracut E. Sections were mounted on carbon coated, Formvar covered copper TEM grids and stained with RuO_4 vapour for 20 min.

3. Results

3.1. Phase morphology prior to tensile pull

The phase morphology of PC–PET blend sections prior to a tensile pull is illustrated schematically in Fig. 3. The PET morphology consists of well defined

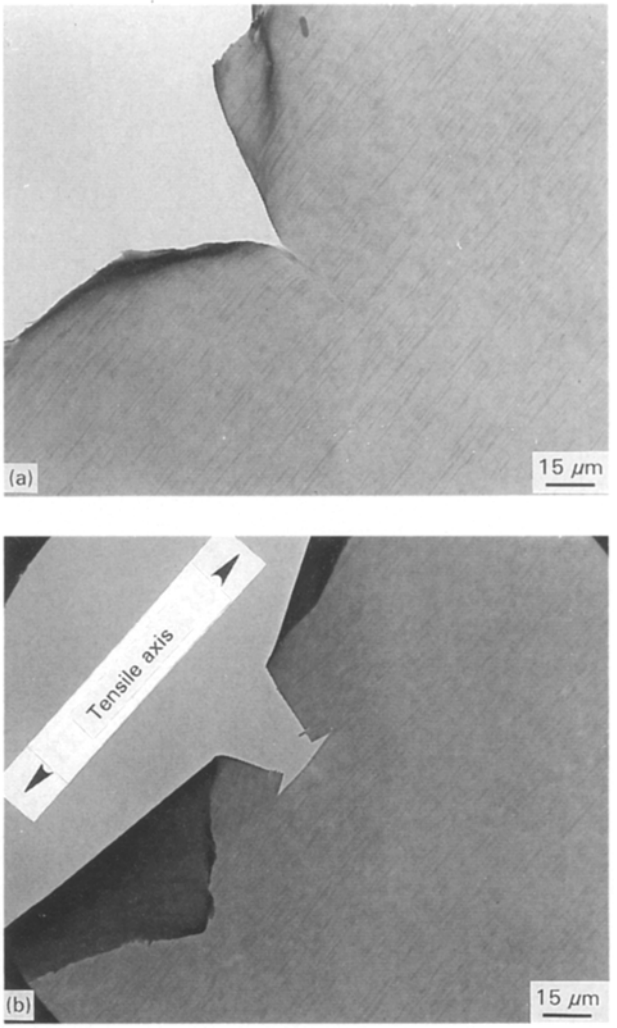

Figure 7 Crack propagation in PC–PET, microtomed parallel to flow with the crack propagation direction perpendicular to the oriented PET rods. The sequence shows (a) the precrack, and (b) advancement of a sharply defined crack to the point where it bisects to go around a long PET domain.

rods, 0.1–1 μm in diameter and 5–45 μm in length. The PET is well known to be only slightly soluble in PC; its solubility parameter being 10.7 versus 9.7 $cal^{1/2}\,cm^{3/2}$ for PC [5]. No occlusions of PC were found in the PET domains. The PET domains were judged to be amorphous by scanning calorimetry and the PC–PET interface appeared smooth at the 30 nm scale. The homopolymers of PC and amorphous PET gave bulk tensile properties of modulus and tensile yield stress as 2.1 GPa, 60 MPa and 1.7 GPa, 45 MPa, respectively. For sections cut perpendicular to flow, disc shaped PET domains are obtained, Fig. 4a. By cutting parallel to the oriented domains PET rods are obtained, Fig. 4b. Fig. 4b illustrates the distribution of shapes and sizes of the rods caused by droplet break up [5].

3.2. *In situ* tensile TEM observations

For PC–PET cut perpendicular to flow (disc shaped PET domains) two types of responses were observed based on the sharpness of the crack tip. A sharp crack is defined as one where the crack tip radius is much smaller than the morphological features (PET discs).

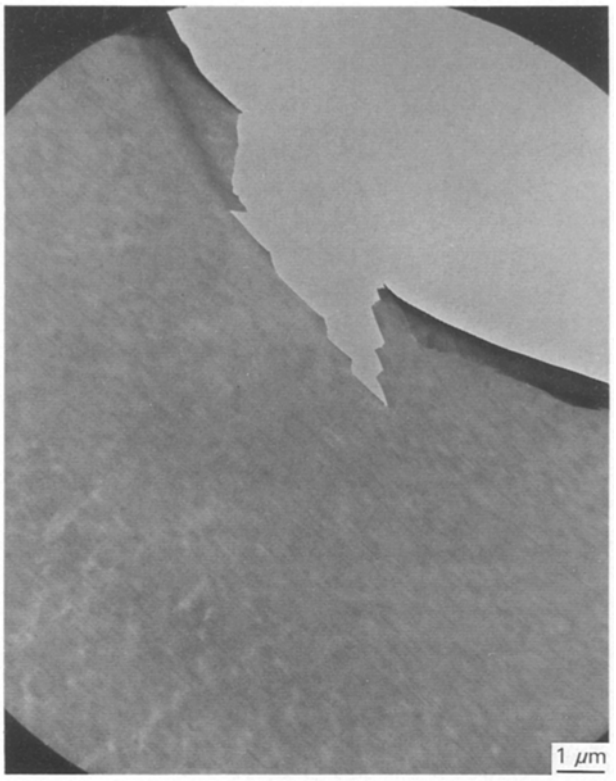

Figure 8 High magnification micrograph of a crack propagating in a section cut parallel to melt flow with the crack propagating perpendicular to oriented PET rods. In this image the crack moves along large PET domains rather than cutting through them, producing a jagged crack surface.

In Fig. 5, the crack tip radius is at the nanometre scale, whereas in Fig. 6 the crack tip radius is at the micrometre scale. The latter blunt crack tip is associated with stable loading conditions. When a slow, blunt crack propagates in this material considerable PET phase distortion and yielding occurs, Fig. 6. The PET domains become elongated during blunt crack propagation. The rate of crack propagation for these two types of cracks was typically different, with the sharp crack moving quicker than the blunt crack for the same rate of the specimen pulling. The slow crack speed is estimated to be 0.1–0.6 $\mu m\,s^{-1}$ and the fast crack speed is 900–1500 $\mu m\,s^{-1}$. Cracks, either sharp or blunt, went around PET domains at slow propagation rates (speed of crack < the rate of pull) and interfacial failure between PC and PET was observed, Fig. 6. However, if the crack propagation is quick (more than the rate of pull) and the crack tip is sharp, the crack will cut right through the domains, Fig. 5. In cases where the crack encountered several PET domains collinear with and several micrometres ahead of the crack tip, failure occurred at the interfaces of these domains.

In Fig. 7a, a precrack is shown oriented perpendicular to the length of the PET rods. When a sharp, slow crack begins to propagate through the section, it moves straight through the PC matrix until it reaches a long PET domain (length greater than about 60 μm) perpendicular to the crack plane. The crack then bifurcates, Fig. 7b, and propagates along the interface of the PET rod. This mechanism again reflects the relatively weak interface between the PC and PET. Consequently, a sawtooth-like path results as the crack moves around PET domains rather than going through them. The evidence of this can be seen in more detail in Fig. 8. Conversely, at high crack speed (quicker than the rate of pull) when the crack was confronted by a large PET domain, the crack was seen to bisect the PET domain rather than going around it.

With the precrack parallel to the direction of PET rods, slow, steady crack propagation was rarely achieved, even at very slow rates of pulling. Failure occurred by a series of rapid crack movements along the PC–PET interface, followed by prolonged blunting and then continued rapid propagation. Fig. 9a shows evidence of the notch blunting following rapid crack growth, Fig. 9b, and an area further into the

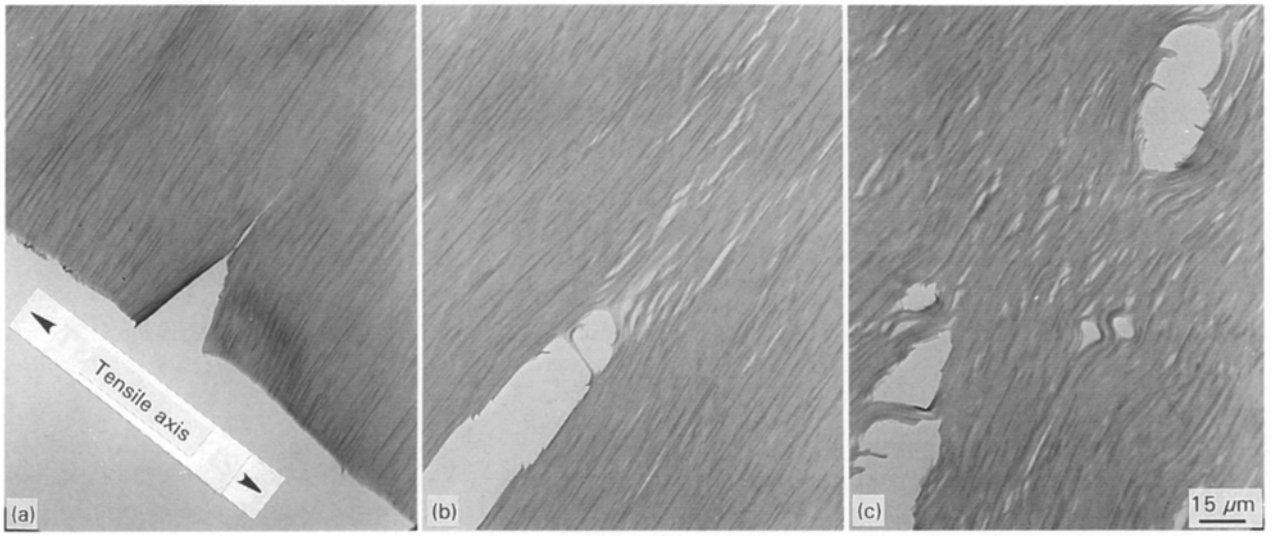

Figure 9 Crack propagation sequence in PC–PET, microtomed parallel to flow with the crack propagation direction parallel to the orientation of PET rods. The sequence shows (a) the precrack, (b) rapid advancement of a sharply defined crack along PET rods, and (c) multiple crack fronts along PET–PC interfaces.

Figure 10 Area in bulk tested PC–PET where the crack stopped when a relatively ductile failure was produced (approach I). The crack integrity was maintained with epoxy for microtomy.

section shows where blunting occurs, followed by failure at several places near and ahead of the crack front, Fig. 9c.

3.3. Post-mortem TEM of cracks propagated in the bulk

Sections were taken from the core of the sample around the crack and crack-tip using epoxy embedding. The crack exhibited many of the features seen in the *in situ*, thin film studies. Fig. 10 shows a mosaic of TEM photos from a relatively ductile crack produced using approach I. In agreement with *in situ* TEM studies for a rapidly moving crack, a number of PET domains appear to have been bisected. Cavitation at the PC–PET interface was observed several micrometres ahead of the notch. Fig. 11 displays a mosaic of TEM pictures representing relatively brittle crack growth produced using approach II. It is evident that the PET domains surrounding the crack are highly elongated due to shear yielding of the PC matrix associated with this type of crack growth. In several instances similar failure mechanisms have been observed for both bulk tested and *in situ* TEM studies.

4. Discussion

The obvious questions to ask relate to the differences in the thickness of the thin film compared to the bulk. In the thin film the PET domains are essentially

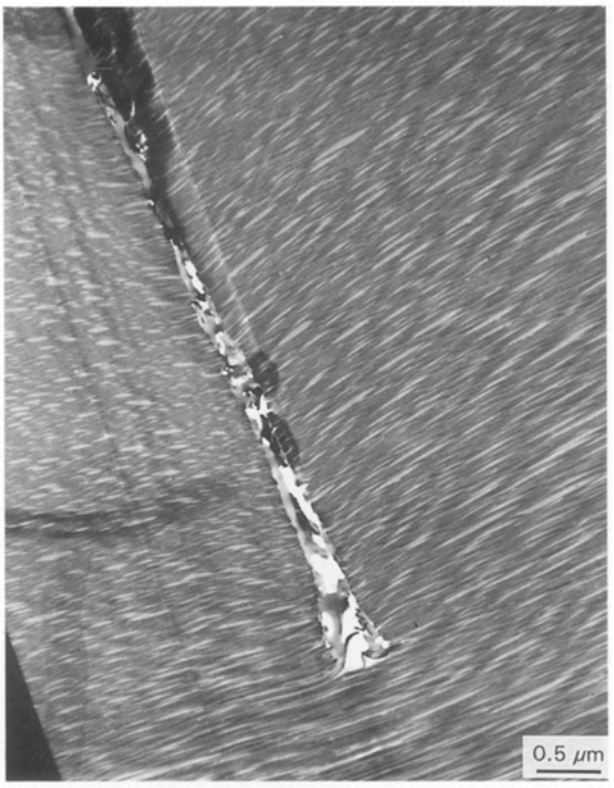

Figure 11 Area in bulk tested PC–PET where the crack stopped for a relatively brittle failure (approach II). The crack integrity was maintained with epoxy.

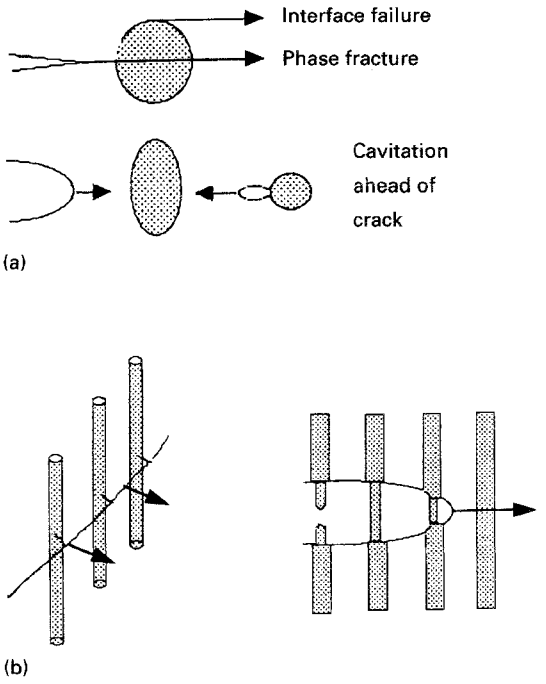

Figure 12 Schematic illustrating failure mechanisms for crack growth in (a) two-dimensional TEM thin-sections and (b) three-dimensional bulk pieces of PC–PET.

two-dimensional and the stress state is considered plane stress. In the core of the bulk specimen the PET domains are three-dimensional and the stress state is mainly in plane strain. In addition, there are complex stress field interactions. In the face of these differences one may wonder why a similarity of failure mechanisms in the thin films and in the bulk was observed at all! An attempt at conciliation is given as follows.

It is clear that in the bulk there is a three-dimensional phase morphology experiencing a crack in a three-dimensional stress state (plane strain at the core and plane stress at the skin). Conversely, in the *in situ* TEM studies of thin-sections a two-dimensional phase morphology is experiencing a crack in a two-dimensional stress state (plane stress). In spite of the expected differences in stress state there are several similarities in failure mechanisms for PC–PET as illustrated in Fig. 12. In two-dimensional crack growth, interfacial failure and phase fracture occur depending on the crack speed. In some instances cavitation was noticed ahead of the crack. In three-dimensional crack growth, similar mechanisms can occur by bisection, interfacial failure around and along the PET rods, or by drawing of the PET rods. This similarity shows that it is instructive to study real time failure to design phase morphology for PC–PET bulk samples.

From the observations in thin film or bulk it appears the "weakest link" in the PC–PET blends is the strength of the PC–PET interface, particularly in tension. Recent studies in the laboratory using four-point bend compression moulded bars of PC–PET bilayers suggest the strength of the interface in tension to be an order of magnitude less than the yield strength [16]. The interesting observation from the bulk studies is that the region between bifurcating cracks appeared to deform to large strains without failure. This suggested that the PC–PET interface strength in shear is greater than the PC and PET yield strength.

Conclusions

1. New techniques for *in situ* transmission electron microscope tensile deformation of polymer films cut from bulk specimens have been developed. The techniques have been applied to examine the micromechanisms of failure of various morphologies of polycarbonate–poly(ethylene terephthalate), PC–PET, blends.

2. The "weakest link" in the strength of these blends was found to be the PC–PET interface, particularly under tension. This enabled cavities to form ahead of the crack tip and the crack to jump through the zone of preformed damage.

3. The rates of crack growth were found to be highly dependent on the orientation and sizes of the PET phases to the applied stress.

4. The apparent mechanisms of crack growth in the bulk PC–PET, examined by post-mortem analysis, were replicated in the thin film *in situ* TEM tensile studies.

Acknowledgements

The collaboration of R. C. Cieslinski in the development of the tensile grids and experimental procedures is gratefully acknowledged. We would also like to

thank H. Pham for sharing information, E. T. Vreeland for printing the micrographs and B. T. Moses for assisting with Instron studies.

References

1. Y. I. NAKAMURA, R. I. HASEGAWA and H. I. KUBOTA, *US Patent No. 3 864 428*, Teijin Ltd. (1975).
2. S. R. MURFF, J. W. BARLOW and D. R. PAUL, *J. Appl. Polym. Sci.* **29** (1984) 3231.
3. H. C. FROMUTH and K. M. SHELL, *US Patent No. 4 264 487*, Rohm and Haas (1981).
4. C. P. BOSNYAK, K. SEHANOBISH and E. G. RIGHTOR, *Amer. Che. Soc. Polym. Prepr.* **33** (1992) 624.
5. L. A. UTRACKI, "Polymer Alloys and Blends, Thermodynamics and Rheology" (Hanser, Munich, 1989) Ch. 1.
6. M. K. LAUGHNER, B. N. HERRON and C. P. BOSNYAK, *US Patent No. 5 124 402*, The Dow Chemical Co. (1992).
7. S. R. SEIBEL, A. MOET, D. H. BANK and K. NICHOLS, Proceedings of SPE Antec (Society of Plastics Engineers, Brookfield, Connecticut, 1993) p. 902.
8. H. J. SUE, E. I. GARCIA-MEITIN, B. L. BURTON and C. C. GARRISON, *J. Polym. Sci. Part B Polym. Phys* **29** (1991) 1623.
9. R. P. KAMBOUR, *J. Polym. Sci.* **D7** (1973) 1.
10. C. MAESTRINI and E. J. KRAMER, *Polymer* **32** (1991) 609.
11. B. D. LAUTERWASSER and E. J. KRAMER, *Phil. Mag. A* **39** (1979) 469.
12. L. BERGER and E. J. KRAMER, *J. Mater. Sci.* **22** (1987) 2739.
13. W. W. ADAMS, D. YANG and E. L. THOMAS, *ibid.* **21** (1986) 2239.
14. A. DONALD and E. J. KRAMER, *ibid.* **16** (1981) 2967.
15. E. G. RIGHTOR, G. P. YOUNG, K. SEHANOBISH, J. C. CONBOY, C. P. BOSNYAK, *ibid.* in press.
16. H. T. PHAM, K. SEHANOBISH, E. G. RIGHTOR, Proceedings of SPE Antec (Society of Plastics Engineers, Brookfield, Connecticut, 1994) p. 1713.

Received 31 January
and accepted 5 August 1994